machines

MDPI

Article

Pool Boiling Performance of a Sintered Aluminum Powder Wick for a Lightweight Vapor Chamber

Liwen Ou [1], Xingchi Jiang [2], Shiwei Zhang [1], Yong Tang [1], Guisheng Zhong [3] and Jie Li [1,*]

[1] School of Mechanical and Automotive Engineering, South China University of Technology, Guangzhou 510640, China
[2] College of Architecture and Environment, Sichuan University, Chengdu 610065, China
[3] Department of Mechanical Engineering, College of Engineering, Shantou University, Shantou 515063, China
* Correspondence: rzlt1314@163.com

Abstract: Aluminum vapor chambers have become an important component used to solve heat dissipation problems in lightweight applications due to their low density and good heat transfer characteristics. In this paper, a new sintered aluminum powder wick is provided for an aluminum vapor chamber. An aluminum porous wick was sintered using liquid phase sintering technology. Using acetone as the working medium, the influence of the structural parameters of the aluminum wick on its boiling heat transfer performance was studied. The influence of thickness on the boiling heat transfer performance of a sintered porous wick is particularly significant. Thinner, porous wicks have better critical heat flux (CHF). The porosity and particle diameter mainly affect the heat transfer coefficient (HTC). At a low heat flux, the sintered wick with low porosity and a small particle diameter has a higher HTC. The HTC of porous wicks, with a larger particle diameter and porosity, decreases slower. The optimal porosity ranges from 46.4 ± 2.5% to 51.8 ± 2.5%. Compared with the polished aluminum plate, the CHF is increased by 1.7 times, and the HTC is increased by about 4.6 times under the same heat flux.

Keywords: pool boiling; heat transfer enhancement; aluminum vapor chamber; sintered aluminum powder wick

Citation: Ou, L.; Jiang, X.; Zhang, S.; Tang, Y.; Zhong, G.; Li, J. Pool Boiling Performance of a Sintered Aluminum Powder Wick for a Lightweight Vapor Chamber. *Machines* **2023**, *11*, 468. https://doi.org/10.3390/machines11040468

Academic Editor: Mohamed S. Gadala

Received: 1 March 2023
Revised: 17 March 2023
Accepted: 21 March 2023
Published: 11 April 2023

1. Introduction

With the development of space technology, heat dissipation has become an urgent problem that requires solving. Vapor chambers are widely used in heat dissipation. Most vapor chambers are made of copper- or aluminum-based materials. Aluminum vapor chambers are important to solving the heat dissipation problem of aerospace devices due to their high heat transfer performance, wide operating temperature zone, and lightweight characteristics. The wick structure is the core component of an aluminum vapor chamber. It is the decisive factor in improving the heat transfer coefficient and ultimate cooling power of the vapor chamber. In previous studies, the wick of the aluminum vapor chamber mainly consisted of a groove and aluminum wire mesh [1,2]. However, these wicks are often unable to meet the high heat flux heat dissipation requirements due to limitations, such as low capillary pressure, high phase transition nucleation superheat, and smaller nucleation core.

Xie et al. [3] summarized several important factors regarding the effect of wick structure on the performance of vapor chamber heat transfer and common strategies for improvement. Studies have shown that sintered porous wicks have a large capillary pressure and a low manufacturing cost, which are key to solving the above problems. However, there are few studies that involve the sintering of aluminum powder. This may be because there is an alumina layer on the surface of the aluminum, which prevents the aluminum powder from sintering. On the other hand, there have been many studies concerning the sintering of copper powder or other aluminum-based wicks [1,2,4–9].

Many scholars have studied the influence of surface morphology and other parameters on the boiling performance of sintered copper powder wicks. Ji et al. [4] studied the pool boiling heat transfer process under the normal pressure of acetone and prepared seven kinds of boiling surfaces. They tested the effect of porous structure on the wick and channel on steam escape. It was found that the 2D and 3D porous surfaces significantly enhanced the boiling heat transfer. Liter et al. [5] compared the influence of cylindrical and tapered porous surfaces on CHF. It was found that the CHF on the surface of one of the conical porous structures increased by two times. The hypothesis was put forward that the conical porous structure reduces the disturbance to the liquid channel when the steam escapes. At the same time, the porous structure can delay the collapse of the liquid channel. As a result, the CHF is increased. Xu et al. [6] studied the influence of copper foam with different porosities on the bubble release mode of pool boiling. Moreover, the effect of porosity on boiling heat transfer performance is discussed. Weibel et al. [7] studied the influence of the thickness and particle diameter of a copper powder sintered wick on the boiling performance of the wick. The results show that for a given sintered powder wick thickness, there exists an optimal particle diameter with the minimum thermal resistance due to the mutual restriction of heat transfer area and steam overflow resistance.

Other scholars have studied the effect of aluminum wire mesh and groove wick on boiling heat transfer performance. Zhang et al. [1] sintered aluminum fiber and an aluminum wire mesh in the cavity of an ultra-thin aluminum vapor chamber as the wick. An ultra-thin aluminum flat vapor chamber with a thickness of only 1.5 mm was manufactured. At the same time, the thermal response characteristics of aluminum vapor chambers were studied. The research shows that the flat aluminum vapor chambers with no wick have better thermal response characteristics under the condition of a large dip angle of 90 degrees, while the vapor chambers with wick are more advantageous under the condition of a small dip angle (30° or 60°) due to the enhanced liquid reflux. The boiling heat transfer performance of vapor chambers with an aluminum wick can be improved with surface treatment. Zhong et al. [2] proposed a method to improve the aluminum groove vapor chamber through ultrasonic processing. In the aluminum vapor chamber with acetone as the working medium, the capillary property of the wick increased by an order of magnitude. At the same time, the maximum capillarity height increased by three times. Huang et al. [8] carried out alkali corrosion treatment on the groove aluminum heat pipe to form a tiny, rough structure on the aluminum surface. The capillary properties of the aluminum groove vapor chamber were significantly improved. The optimum corrosion time and concentration were also studied. Based on this research, a heat pipe heat transfer limit prediction method based on capillary rise rate is proposed. Zhang et al. [9] developed a hierarchical gradient mesh surface that exhibited an exceptionally high CHF of 300 W/cm^2 and HTC of 34.52 W/(cm^{2}K), which are 313% and 811% larger than those of the plain surface with deionized water under 1 atmosphere pressure. By simply sintering multilayer meshes with a controllable porosity and a superhydrophilic micro/nanostructured coating, the surface developed is cost-effective and capable of exhibiting a strong wicking effect and rapid small bubble detachment characteristics via a chimney-like architecture.

However, the aluminum wicks mentioned above have the disadvantages of low capillary pressure, high phase transition nucleation superheat, and a smaller nucleation core. Therefore, some scholars have studied the manufacturing method of sintering the wick of aluminum powder [9–17]. Ameli et al. [10] sintered aluminum powder using a selective laser melting process (SLM) to develop a porous structure composed of many octahedral elements. This method was used to produce a series of wick structures with different thicknesses, porosities, and pore sizes. Wu et al. [11] prepared the nanostructures of the coated surface of gold nanoparticles and the coated surface of alumina nanoparticles using electrophoretic deposition technology. The effects of nanoparticle mass, the size and materials of nanoparticles, as well as the solvents and working media in the process of electrophoretic deposition on the boiling heat transfer were studied. Compared with the smooth surface, the HTC of pool boiling increased by 80%. Schaffer et al. [12] studied the

sintering behavior of aluminum powder mixed with different elements. It was found that adding trace magnesium to produce spinel can break the oxide layer on the surface of aluminum powder and promote the sintering of aluminum powder. Godinez et al. [17] studied the effects of an aluminum high-temperature conductive microporous coating on the nucleate boiling heat transfer coefficient and critical heat flux in saturated distilled water at 1 atm. The aluminum high-temperature conductive microporous coating was shown, experimentally, to improve the nucleate boiling heat transfer coefficient by a factor of five as the wall superheat was reduced by from 31 K to 6 K just before CHF.

In this paper, liquid phase sintering technology was used to manufacture the sintered aluminum powder wick. The aim of this study is to explore the effect of the parameters of the sintered wick on the boiling performance. Therefore, an aluminum powder sintered wick with gradient changes in thickness, porosity, and particle diameter was manufactured. After conducting a wettability test and carrying out a pool boiling experiment, the boiling curve and heat transfer coefficient of the sample were compared. Finally, the optimum parameters for sintering aluminum powder were obtained.

2. Experiment

2.1. Sample Preparation

In this study, liquid phase sintering manufacturing technology is used to sinter the aluminum powder wick. Pure aluminum powder is used as the base material. AlSi10Mg aluminum alloy powder was mixed with pure aluminum powder as filler metal powder. The mixed powder was spread in the fixture, and the loose sintering method was used for manufacturing the aluminum-based wick, as shown in Figure 1. Due to the active chemical properties of aluminum, the sintering of aluminum powder was carried out in a vacuum furnace. The sintering temperature of the aluminum powder was increased from its normal temperature to 615 °C and kept for 10 min. The sintered aluminum powder wick is shown in Figure 2a. Adjusting the ratio of aluminum and aluminum alloy powder can control the aluminum powder sintering wick. The particle diameter and thickness of the sample can be easily changed by using different particle diameter aluminum powder or changing the thickness of the mold. The experimental samples manufactured in this study are shown in Table 1 below. In this paper, polished aluminum plates are also used for boiling heat transfer tests, as shown in Figure 2b, which presents an SEM image of the surface of the polished aluminum sheet. It can be seen that there are still some scratches and pits on the surface of the polished aluminum sheet after grinding, which has a partial influence on the boiling performance. The surface morphology of the sintered aluminum powder wick is shown in Figure 2c,d. There is a dense oxide film on the surface of the aluminum powder to hinder the sintering of aluminum powder. It can be verified that the adjacent aluminum powder particles join together, indicating that aluminum powder sintering was successful.

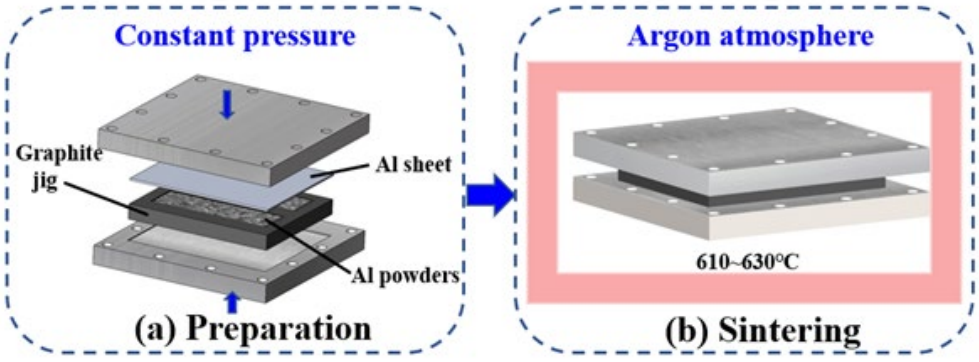

Figure 1. Preparation method of sintered aluminum powder wick.

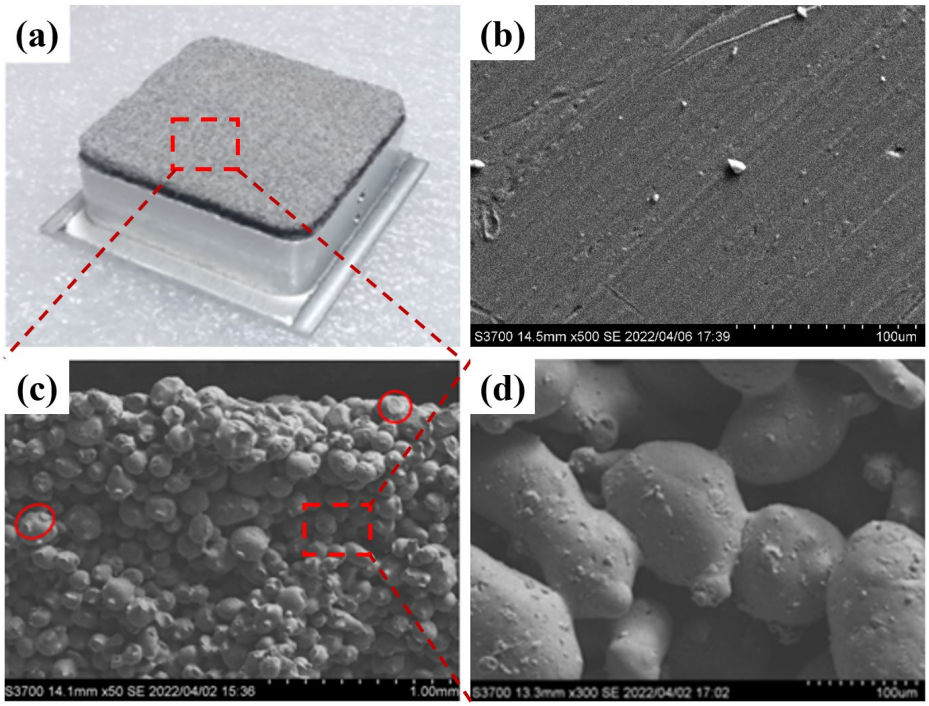

Figure 2. Image of aluminum wick: (**a**) Photos of sintered aluminum powder wick; (**b**) SEM image of polished aluminum plate; (**c**,**d**) SEM image of sintered aluminum powder wick.

Table 1. Experimental sample parameters.

Sample	Porous Thickness	Porosity	Particle Diameter
D6P3-05	0.5 mm	38.2 ± 2.5%	60 μm
D6P4-05	0.5 mm	46.4 ± 2.5%	60 μm
D6P5-05	0.5 mm	51.8 ± 2.5%	60 μm
D6P6-05	0.5 mm	57.2 ± 2.5%	60 μm
D13P3-05	0.5 mm	38.2 ± 2.5%	132 μm
D13P4-05	0.5 mm	46.4 ± 2.5%	132 μm
D13P5-05	0.5 mm	51.8 ± 2.5%	132 μm
D13P6-05	0.5 mm	57.2 ± 2.5%	132 μm
D13P4-10	1 mm	46.4 ± 2.5%	132 μm
D13P4-20	2 mm	46.4 ± 2.5%	132 μm

2.2. Test for Wettability

In this paper, the wettability of the sintered wick with water and alcohol is studied to distinguish the wettability of samples with different sintering parameters. The main parameters affecting the performance of the aluminum powder sintered wick are porosity and particle diameter. The wetting process of the aluminum powder sintered wick with different parameters was recorded using a high-speed camera. Figure 3 shows the spreading process of water and ethanol on the surface of sample D6P4-05.

The droplet spreading time of other samples is shown in Figure 4. The porosity of the sintered wick increased from 38.2 ± 2.5% to 57.2 ± 2.5% (P3 to P6). It can be seen that under the condition of the same porosity, the sintered wick of aluminum powder with a particle diameter of 60 μm has better wettability. When the particle diameter is 132 μm, the spread time of droplets increases rapidly with the increase in porosity. When the particle diameter is 60 μm, the spreading time is shortened with a decrease in porosity when the porosity is higher than 46.4 ± 2.5%. However, when the porosity decreases to 46.4 ± 2.5%, the droplet spreading time increases. When the porosity is too small, the void volume of the sintered liquid core is limited, and the viscous resistance increases after water droplets

occupy part of the volume, resulting in the slowing down of water flow. This may be the result of the influence of the size of the gas escape channel and the capillary force on the droplet spreading speed.

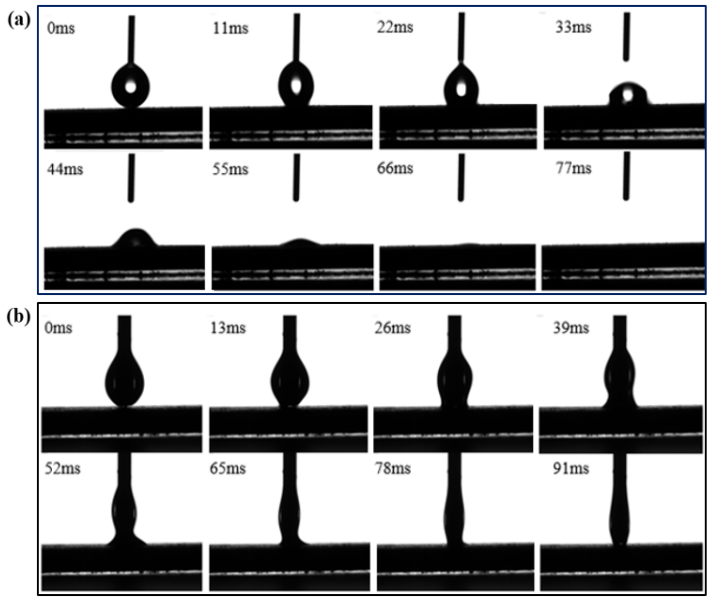

Figure 3. Spreading process of different working media on the surface of D6P4-05. (**a**) water, (**b**) ethanol.

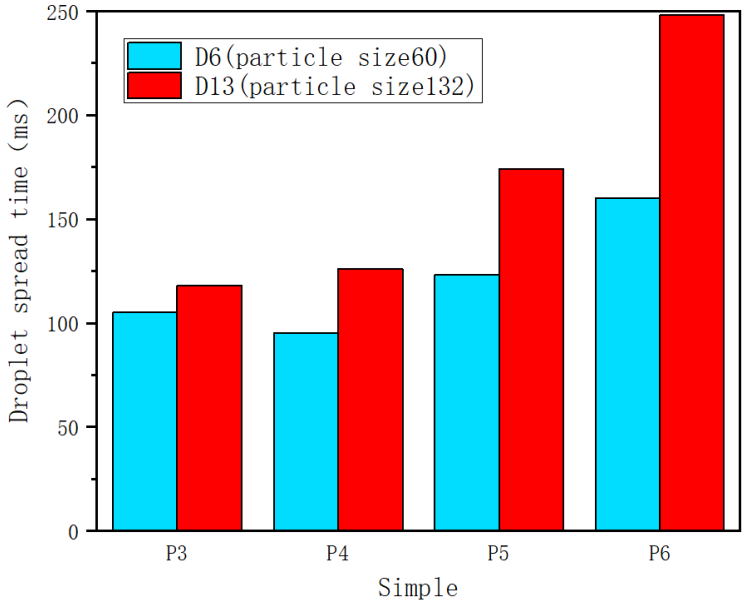

Figure 4. Droplet spreading time of samples with different parameters.

2.3. Pool Boiling Apparatus and Data Reduction

Figure 5 shows the pool boiling test device used in this study. This device is composed of a liquid container, a heating system, a liquid temperature control device, a data acquisition system, and a high-speed camera system. The experimental process was recorded by a high-speed camera. The walls of the container are made of transparent quartz glass, so that the formation and detachment of bubbles can be easily observed and recorded. The bottom of the container is sealed with sealant. A liquid temperature control device was used to heat and maintain the temperature of the liquid. The heating system is made of copper blocks. A sintered aluminum powder wick was sintered onto an aluminum block.

The aluminum block was clamped to the surface of the heated copper block during the test. Liquid metal was applied between the aluminum block and the heated copper block to reduce thermal resistance. It was installed at the bottom of the container and sealed with sealant. The heating surface size is 25 mm × 25 mm, which is the same as the sample size. The heat of the copper block is provided by 9 resistance heating rods. The maximum power of each heating rod is 80 W. The heating system can supply the maximum heating power of 720 W. The power of the heating system was monitored and controlled by transformer and wattmeter. There are 6 T-type thermocouples on the heating system. Thermocouple T1 is 3.0 mm away from the bottom of the sintered aluminum powder wick. The thermocouple T1 could directly measure the temperature at the bottom of the sintered aluminum powder wick. Therefore, the influence of the thermal resistance of the interface between copper and aluminum blocks on the experimental data could be ignored. The other thermocouples T3, T4, T5 and T6 are vertically arranged below T1 at 6.0 mm intervals. The thermocouple data were recorded in real time by the data acquisition card and the computer.

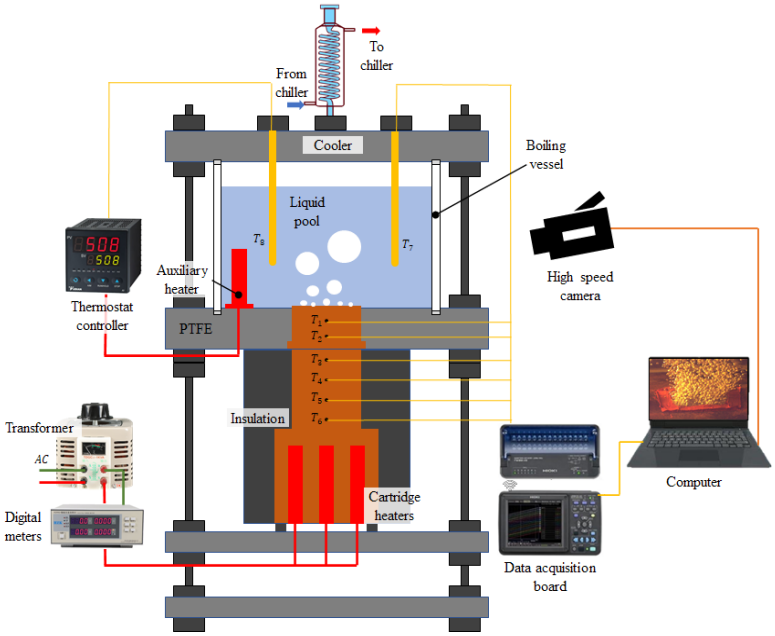

Figure 5. Experimental apparatus for pool boiling.

When the heat loss from the surrounding area is negligible, the sample heat flux and wall superheat can be calculated by Fourier's law. In order to determine whether Fourier's law is valid, the temperature distribution of the device under different heat fluxes was tested, as shown in Figure 6. The temperatures of four positions T3–T6 were selected for fitting, as shown in Figure 6. Adj.R^2 is 0.999, 0.998, 0.999 and 0.999, respectively. It can be seen that Adj.R^2 is not less than 0.998, indicating a linear distribution of temperature. The heat flux can be obtained by the following formula:

$$q'' = -k_{Cu}\frac{T_6 - T_3}{3x_2} \tag{1}$$

where k_{Cu} is the thermal conductivity of copper, and x_2 = 6 mm is the distance between two adjacent thermocouples. The boiling surface temperature T_w can be calculated as follows:

$$T_w = T_1 - q''\left(\frac{x_1}{k_{Cu}} + \frac{t_s}{k_s}\right) \tag{2}$$

where x_1 = 3 mm is the distance between the thermocouple T_1 and the heating block, t_s is the thickness of the solder layer, and k_s is the thermal conductivity of the solder layer.

The wall superheat ΔT is the difference between the wall temperature and the surrounding acetone temperature, and can be obtained as:

$$\Delta T = T_w - T_a \tag{3}$$

in which T_a is the temperature of the surrounding acetone measured by thermocouple T_7. Then, the boiling heat transfer coefficient (h) can be obtained as:

$$h = \frac{q''}{\Delta T} \tag{4}$$

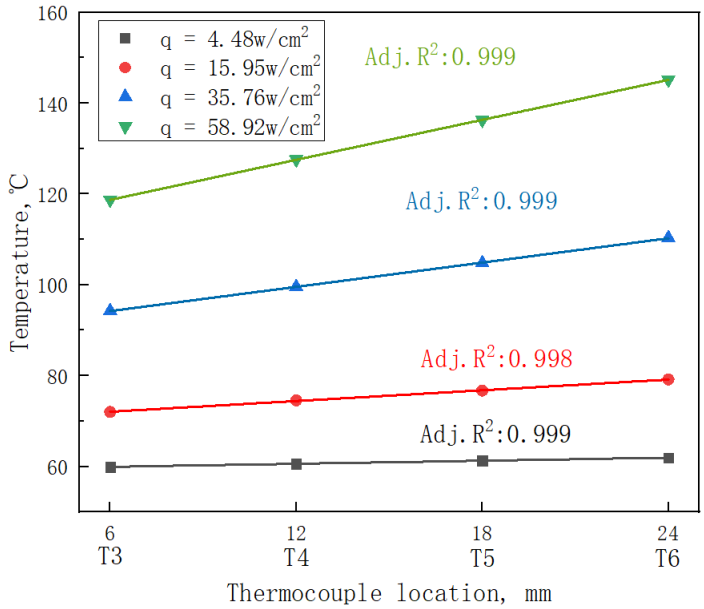

Figure 6. Heat flux regression curves of the device.

The uncertainty of the whole test system can be estimated by the standard error analysis method, as shown in Equations (5) and (8). The measurement uncertainty of the T-type thermocouple is ± 0.2 °C. The location uncertainty for those thermocouples is estimated as ± 0.05 mm. The uncertainty of the thickness of the solder layer t_s is less than 2%. The uncertainty of the heat flux is estimated to be less than 6.37%. The uncertainty of HTC is estimated to be less than 8.26%.

$$\frac{U_{q''}}{q''} = \left[\left(\frac{U_{T_6}}{T_6 - T_3}\right)^2 + \left(\frac{U_{T_3}}{T_6 - T_3}\right)^2 + \left(\frac{U_{x_2}}{x_2}\right)^2\right]^{1/2} \tag{5}$$

$$\frac{U_{T_w}}{T_w} = \left\{\left(\frac{U_{T_1}}{T_w}\right)^2 + \left[\left(\frac{x_1}{k_{Cu}} + \frac{t_s}{k_s}\right)\cdot\frac{U_{q''}}{T_w}\right]^2 + \left(\frac{q'' U_{x_1}}{T_w k_{Cu}}\right)^2 + \left(\frac{q'' U_{t_s}}{T_w k_s}\right)^2\right\}^{1/2} \tag{6}$$

$$\frac{U_{\Delta T}}{\Delta T} = \left[\left(\frac{U_{T_w}}{\Delta T}\right)^2 + \left(\frac{U_{T_a}}{\Delta T}\right)^2\right]^{1/2} \tag{7}$$

$$\frac{U_h}{h} = \left[\left(\frac{U_{q''}}{q''}\right)^2 + \left(\frac{U_{\Delta T}}{\Delta T}\right)^2\right]^{1/2} \tag{8}$$

3. Results and Discussion

3.1. Verification of Device Accuracy

In order to verify the accuracy of the pool boiling test device, the pool boiling performance of a polished aluminum plate was tested first. The results were compared with the theoretical results of Rohsenow [13]. It is believed that the main heat transfer mode of boiling is the efficient heat transfer between a solid and liquid caused by a violent disturbance in the process of bubble separation. The following formula for calculating the heat transfer of pool boiling is proposed:

$$\frac{c_{pl} \cdot \Delta T_{sat}}{h_{lv}} = C_{sf}\left[\frac{q_a}{\mu \cdot h_{lv}}\sqrt{\frac{\sigma}{g(\rho_l - \rho_v)}}\right]^{0.33}\left(\frac{c_{pl} \cdot \mu}{k_l}\right)^n \quad (9)$$

Among them, c_{pl}, h_{lv}, μ and σ are the specific heat capacity, latent heat of vaporization, dynamic viscosity and surface tension of liquid at atmospheric pressure, ρ_l and ρ_v are the density of liquid and vapor. The k_l is the thermal conductivity of liquid working medium. The C_{sf} and n are the dimensionless empirical constant and empirical index, respectively. In this study, the solid-liquid combination of aluminum and acetone is used. Their values are 0.0096 and 1.7 [14], respectively.

The experimental results and calculation results of the polished aluminum plate are shown in Figure 7. At a low heat flux, the experimental boiling curve of the aluminum plate basically coincides with the theoretical calculation results of Rohsenow. At a high heat flux, the experimental boiling curve of the aluminum plate deviates to the left. The maximum deviation is still less than 3 °C. This deviation is mainly affected by the rough surface. Scratches and pits on the surface of the polished aluminum, as shown in Figure 2b, improve the wettability of the aluminum and allow bubbles to escape the boiling surface more easily. In addition, scratches enhance the horizontal complement of the working medium. This results in a lower superheat of the polished aluminum plate than the theoretical value at high heat flux. It can be seen from Figure 7 that the boiling measuring device has a high accuracy within the range of the measured heat flux.

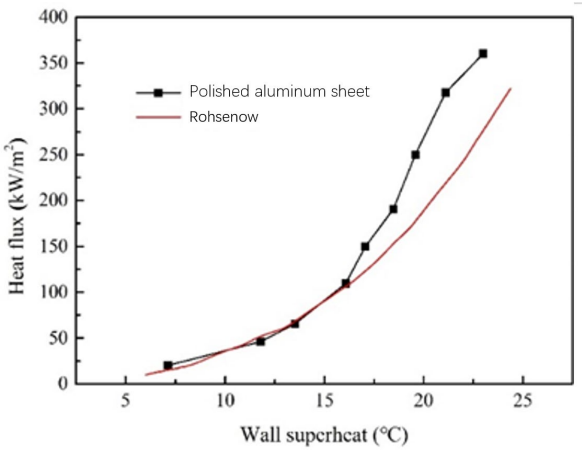

Figure 7. Acetone pool boiling test curves on the surface of an aluminum plate.

3.2. Effect of Thickness on Boiling Performance

Figure 8 shows the boiling curve and boiling HTC of a sintered porous wick of aluminum powder with different thicknesses. Compared with the aluminum plate, it can be seen that the wall superheat of the sintered porous wick of aluminum powder is significantly reduced. At the same heat flux, sample D13P4-05 has the lowest wall superheat. Its maximum value is only 11.3 °C. With the increase in the sintered thickness of aluminum powder, the boiling curve gradually shifted to the lower right. It may be that the wall superheat gradually increased. This indicates that the enhanced boiling heat transfer performance of the sintered porous wick of aluminum powder gradually weakened with

the increase in the thickness. With the increase in sintering thickness, the CHF of aluminum powder decreased gradually. The results show that the CHF of the porous structure is the largest at the sintered thickness of 0.5 mm. The CHF decreased greatly in the range of 0.5~1 mm. When the thickness exceeds 1 mm, the decrease in the CHF is significantly reduced. The HTC under a low heat flux density and the HTC of a sintered aluminum powder wick are not far apart, not less than 20 kW/(m^2·K). It is significantly higher than that of the aluminum plate (3.9 kW/(m^2·K)), and rapidly increases with the increase in heat flux. When the heat flux density increases, the HTC of sample D13P4-05 first tends to exhibit a stable rise after the fall. When the heat flux is 443.1 kW/m^2, the HTC reaches the maximum value of 61.9 kW/(m^2·K). For samples D13P4-10 and D13P4-20, the HTC gradually decreases or becomes gentle with the increase in heat flux. This indicates that the enhanced boiling heat transfer performance of samples D13P4-10 and D13P4-20 gradually weakens at high heat flux. D13P4-10 and D13P4-20 have the highest HTC at 35.6 kW/m^2 and 61.3 kW/m^2, respectively. The main reason for the above phenomenon is that at low heat flux, the porous structure contributes to bubble nucleation. The boiling performance is significantly improved compared with the flat plate. With the increase in heat flux, the thicker porous structure layer will prevent bubbles from escaping, resulting in decreased heat transfer performance. At the same time, bubbles trapped in the porous structure further hinder the supplement of liquid working medium, leading to the decrease in CHF. When the porous layer is thinner, the liquid replenishment efficiency is higher because the formation and separation of bubbles are easier. Finally, the sample obtained better comprehensive boiling heat transfer performance. In conclusion, the porous wick sintered with 0.5 mm thickness of aluminum powder has the best heat transfer performance.

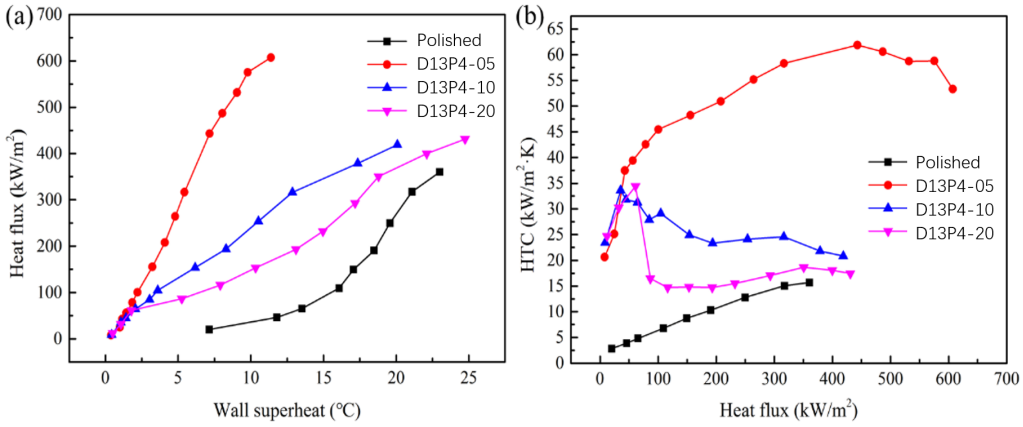

Figure 8. Different thickness of aluminum powder sintered porous wick: (**a**) boiling curve, (**b**) boiling heat transfer coefficient.

3.3. Effects of Particle Diameter and Porosity

The boiling curves of the sintered porous wick with particle diameters of 60 μm and 132 μm are shown in Figures 9 and 10. At low heat flux, the wall superheat of the sintered wick of aluminum powder with different porosities is basically similar, which is much lower than that of the aluminum plate. The results show that the sintered porous wick with different porosities has a similar promoting effect on the bubble growth at low heat flux. The wall superheat required by the activation of the bubble nucleation site on the porous structure is relatively low. In addition, compared with 132 μm, the wall superheat of the 60 μm aluminum powder sintered porous wick is relatively smaller. The difference between different porosities is smaller. With the increase in heat flux, the wall superheat gradually increases. The difference of wall superheat in porous wicks sintered by aluminum powder with different porosities gradually appears. For the 60 μm aluminum powder sintered porous wick, the wall superheat of sample D6P5-05 is relatively low at the same heat flux. This indicates that the porous structure with a porosity of 51.8 ± 2.5% has a relatively strong

promoting effect on bubble nucleation and a relatively high bubble nucleation efficiency at high heat flux. For the 132 μm aluminum powder sintered porous wick, the wall superheat of the porous structure with a porosity of 46.4 ± 2.5% is relatively lower. It may be that the optimal porosity is conducive to decreases in bubble nucleation with the increase in the aluminum powder particle diameter. At the same time, the sintered porous wicks of the aluminum powder with the same particle diameters and different porosities have similar limiting heat flux. For example, the CHF of D6P5-05 and D6P6-05 is 636.3 kW/m^2 and 626.4 kW/m^2. The CHF of D13P5-05 and D13P6-05 is 645.8 kW/m^2 and 607.9 kW/m^2. The results show that under the condition of a certain thickness, the porosity and particle diameter of the porous structure have little influence on the boiling limit heat flux.

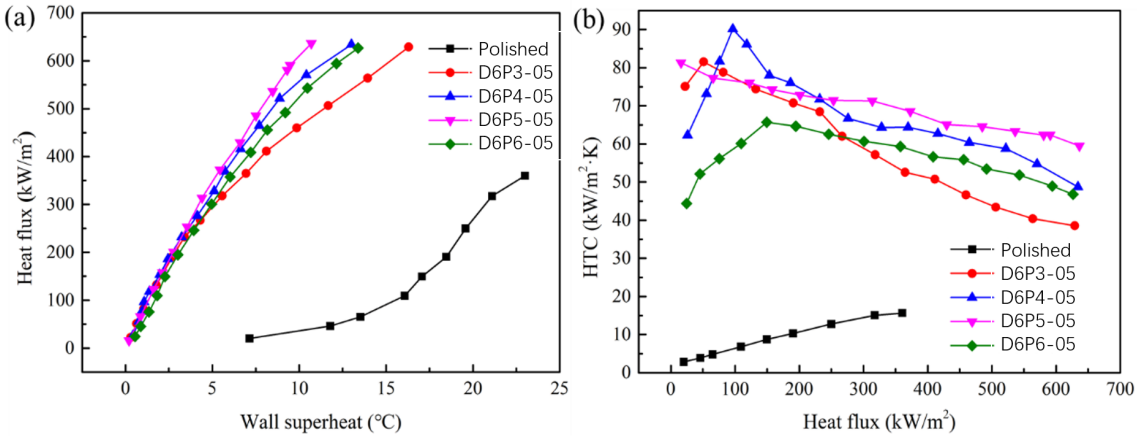

Figure 9. Sintered porous wick with different porosities (particle diameter 60 μm): (**a**) boiling curve, (**b**) boiling heat transfer coefficient.

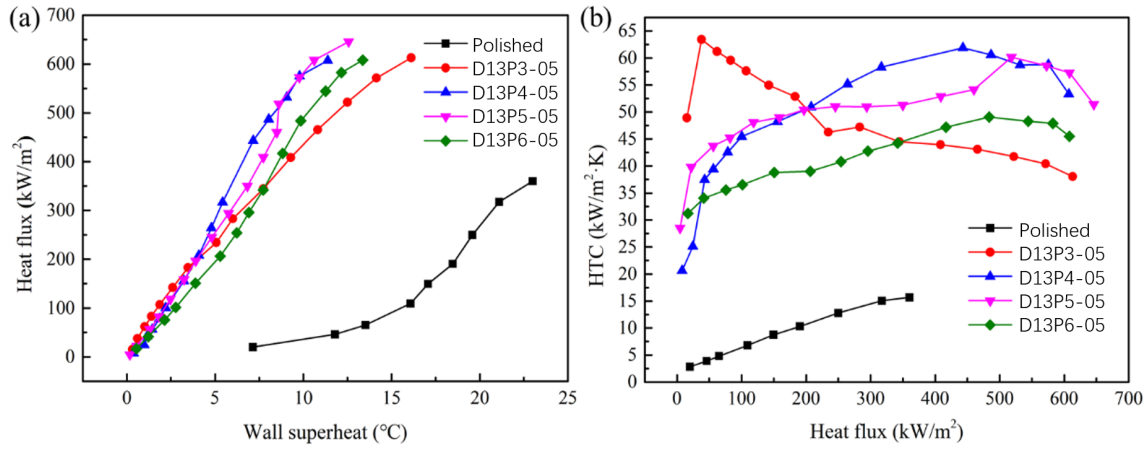

Figure 10. Sintered porous wick with different porosities (particle diameter 132 μm): (**a**) boiling curve, (**b**) boiling heat transfer coefficient.

The HTC of the sintered porous wick with particle diameters of 60 μm and 132 μm is shown in Figures 9b and 10b. The results show that the HTC decreases with the increase in heat flux for the sintered porous wick with a particle diameter of 60 μm. Relatively, D6P5-05 has a high HTC with a value of 81.3~59.4 kW/(m^2·K). The results indicate that the boiling-enhanced heat transfer performance of the porous wick sintered with 60 μm aluminum powder decreased with the increase in heat flux. In the boiling process of high heat flux, large bubbles will be generated. When the pore size is small, the detachment resistance of bubbles is relatively large. The detachment efficiency of bubbles decreases, leading to the decline in the overall boiling heat transfer performance. Therefore, the decrease in the HTC of the 60 μm aluminum powder sintered porous wick at high heat flux may be due to the

small pore size, which leads to the blockage of large bubble escape. The HTC of D6P5-05 decreases more slowly and is higher than that of other samples at high heat flux. These results indicate that D6P5-05 provides a large number of nucleation sites while leaving relatively large channels for bubble escape. The porous structure D13P3-05 sintered with aluminum powder with a particle diameter of 132 μm has the same variation trend. This result shows that the bubble escape resistance in the porous structure with a large particle diameter and low porosity is relatively large at high heat flux, leading to the decrease in boiling heat transfer performance. For the sample with a particle diameter of 132 μm, the HTC increased with the increase in heat flux. When the heat flux density is less than 200 kW/m^2, D13P3-05 has a relatively large HTC, at a value of 48.9~63.4 kW/(m^2·K). When the heat flux density is higher than 200 kW/m^2, HTC of D13P4-05 is relatively large. This result shows that the low porosity of the aluminum powder improved the performance of the enhanced-boiling heat transfer sintered porous wick. The main reason is that the porous structure with larger porosity has a lower pore density and larger pore size, resulting in less density of the corresponding bubble nucleation site and a weak enhancement effect on boiling heat transfer. The HTC of the sintered porous wick with a particle diameter of 60 μm is higher than that with particle diameter of 132 μm, which can be seen by comparing the HTC of different particle diameters. There are more nucleation sites on the sintered porous aluminum powder wick of with a small particle diameter, which has a better enhancement effect on the boiling heat transfer process.

In summary, the sintered porous wicks of aluminum powder with different particle diameters and porosities have lower CHF. The influence of particle diameter and porosity on HTC is significant. At low heat flux, the sintered porous wicks with low porosity and small particle diameter are more conducive to enhancing boiling heat transfer. At high heat flux, the samples with large particle diameters and high porosities have a higher HTC. The optimal porosity range is 46.4 $\pm$ 2.5% to 51.8 $\pm$ 2.5%.

3.4. Bubble Generation Visualization

In this study, a high-speed camera with 3000 frames per second was used to record the bubble growth during the boiling heat transfer test of the sintered wick of aluminum powder, as shown in Figure 11. For the three samples, the density of the bubbles increased with the increase in heat flux. This indicates that more and more nucleation sites are activated with the increase in heat flux. When the heat flux further increased to 300 kW/m^2, the bubble growth rate increased and adjacent bubbles began to fuse with each other. Compared with the polished aluminum plate, the porous structure of the sintered wick had better wettability and promoted bubble escape, delaying the arrival of CHF. Compared with the polished aluminum plate, the CHF of the sintered aluminum powder wick was nearly 1.8 times higher. Compared with D6P4-05 and D6P5-05, sample D6P4-05 had more bubble formation when the heat flux was 20 kW/m^2, which indicates that sample D6P4-05 has more nucleation sites. However, when the heat flux reached 200 kW/m^2, the bubbles of D6P5-05 were smaller, indicating that bubbles of D6P5-05 escape more easily. The comparison between Figure 11b,d shows that at low heat flux, D6P5-05 has more and smaller bubbles, which is due to the relatively small porosity of D6P5-05 promoting the escape of bubbles. At high heat flux, d5 and d6 have similar bubble morphology. This is also consistent with the experimental data.

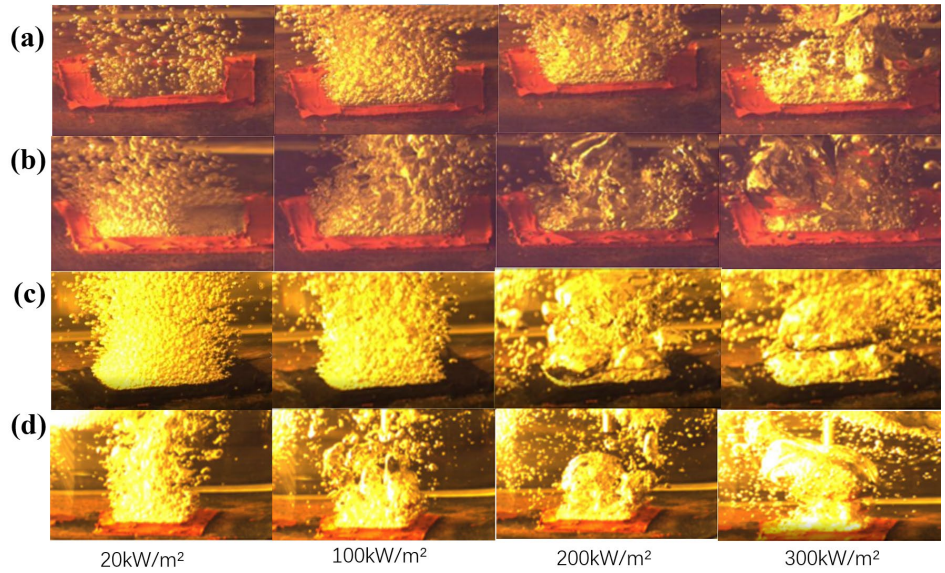

Figure 11. Boiling bubbles on sintered porous wick: (**a**) aluminum plate, (**b**) D6P5-05, (**c**) D6P4-05, (**d**) D13P4-05.

3.5. Comparison with Other Studies

The boiling properties of aluminum powder wicks were compared with those of other studies. Zan Wu's team created a copper-based porous wick, the samples of Electrophoretic Deposition Wick, using the Electrophoretic Deposition method [11]. Then, 1.5 mg copper particles with a particle diameter of 126 ± 24 nm was fixed on the surface of the copper sheet by using electrophoretic deposition technology. Its boiling performance curve is shown in Figure 12. The limiting heat flux of this sample is 32 W/cm^2. When the heat flux is low, the superheat of the electrophoretic deposition wick increases rapidly, which indicates that the activation of the bubble nucleation site of the sample is slow. Compared with D6P5-05, the electrophoretic deposition wick has higher superheat and lower CHF. This may be the reason why the electrophoretic deposition wick has few nucleation sites.

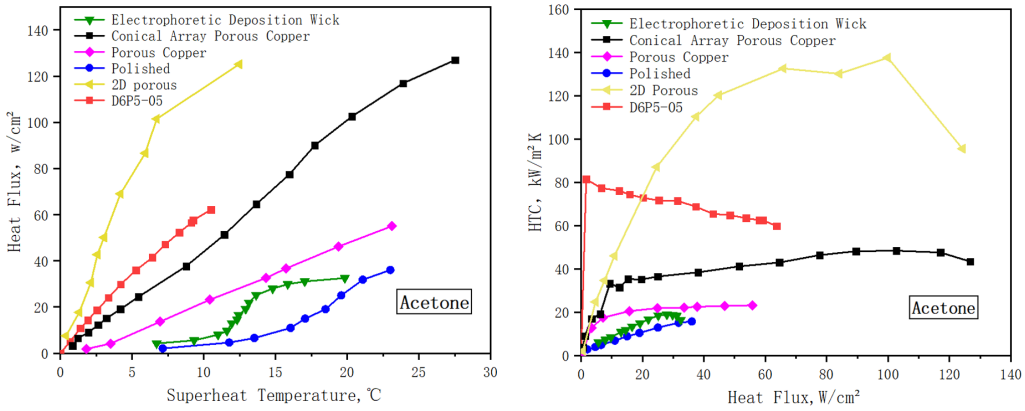

Figure 12. Comparison of heat transfer performance.

Xianbing Ji's team used copper powder at 130–170 nm to form porous wicks with different surface morphologies [2]. The surface of porous copper was covered with a 2.5 mm thick sintered porous layer of copper powder with a porosity of 32%. The surface of sample conical array porous copper was sintered with a 2 mm spaced cone array with a height of 2.5 mm. The surface of 2D porous copper was sintered with a porous structure with a groove shape. Acetone was used as a performance test for these samples. The results are shown in the Figure 12. D6P5-05 and porous copper had lower CHF, but D6P5-05 had

lower superheat and higher HTC. This may be because D6P5-05 has a thinner thickness and bubbles escape more smoothly during the boiling heat transfer process. The CHF of conical array porous copper and 2D porous copper is twice that of D6P5-05. This is because the surface structure of the conical array and 2D porous provide more nucleation sites for bubble growth. At the same time, the structure of the cone with a large bottom and small top also provides a larger channel for bubbles to escape.

4. Conclusions

In this paper, the sintered wick of aluminum powder was fabricated. The boiling heat transfer performance of an aluminum powder wick was studied by conducting the pool boiling experiment. Several main points are concluded below:

(1) Liquid phase sintering technology was used to manufacture the sintered liquid wick of aluminum powder with different parameters. The porosity of the sample ranged from 38.2 $\pm$ 2.5% to 57.2 $\pm$ 2.5%. The alcohol droplets spread rapidly on the samples with all structural parameters. Among them, the sample with a particle diameter of 60 μm and porosity of 46.4% had the best wettability. The droplet spreading time decreased first and then increased with the increase in porosity when the particle diameter was 60 μm. This may be the result of the influence of the size of the gas escape channel and the capillary force on the droplet spreading speed.

(2) The thickness has a significant effect on the boiling heat transfer performance of the sintered wick. When the wick was thick, the boiling heat transfer performance of the sintered wick was poor. As the thickness decreased, the boiling heat transfer performance of the sintered wick had a clear improvement, especially when the heat flux was high. The sintered porous wick with a thickness of 0.5 mm aluminum powder had the best heat transfer performance. This is because the thinner porous layer reduced the travel and resistance of bubbles escaping during the boiling heat transfer process.

(3) The effect of porosity and particle diameter on the HTC is significant. When the particle diameter or the porosity was low, the HTC decreased gradually with the increase in heat flux. At high heat flux, the samples with a large particle diameter and high porosity had a higher HTC. It was found that the boiling heat transfer performance of D6P5-05 is the best. Its CHF of 636.3 kW/m^2 is close to other samples, but its HTC is significantly better than other samples at high heat flux.

(4) The porous structure of the sintered wick greatly improves the boiling heat transfer performance. Compared with the polished aluminum plate, the CHF increased by 1.7 times, and the HTC increased by about 4.6 times at a heat flux of 300 kW/m^2. This is because the porous structure provides more nucleation sites compared with the polished aluminum plate. At the same time, the pores between the aluminum powder provide adequate channels for bubbles to escape.

Author Contributions: Conceptualization, L.O., S.Z. and J.L.; methodology, L.O., S.Z., X.J. and J.L; validation, L.O., G.Z. and J.L.; investigation, Y.T., G.Z. and X.J.; data curation, L.O.; writing—original draft preparation, L.O.; writing—review and editing, J.L.; visualization, L.O. and J.L.; supervision, Y.T. and S.Z.; project administration, S.Z.; funding acquisition, S.Z. All authors have read and agreed to the published version of the manuscript.

Funding: This work was supported by National Natural Science Foundation of China (No. 52105444, 52235011 and U22A20194), Natural Science Foundation of Guangdong Province (2022A1515010375), and S&T Innovation Projects of Zhuhai City (ZH01110405180034PWC).

Institutional Review Board Statement: Not applicable.

Informed Consent Statement: Not applicable.

Data Availability Statement: Data underlying the results presented in this paper are available from the corresponding authors upon reasonable request.

Conflicts of Interest: The authors declare no conflict of interest.

Nomenclatures

CHF	critical heat flux, kW/m^2
HTC(h)	heat transfer coefficient, kW/ (m^2·K)
q''	heat flux, kW/m^2
T_w	wall temperature, °C
k_{Cu}	thermal conductivity of copper, W/ (m·K)
k_s	thermal conductivity of solder, W/ (m·K)
x_1	the distance between T_1 and the top of copper block, mm
x_2	the distance between adjacent thermocouples, mm
T_a	the temperature of surrounding acetone, °C
ΔT	wall superheat, °C
t_s	the thickness of the solder layer, mm

References

1. Zhang, S.; Chen, J.; Sun, Y.; Li, J.; Zeng, J.; Yuan, W.; Tang, Y. Experimental study on the thermal performance of a novel ultra-thin aluminum flat heat pipe. *Renew. Energy* **2018**, *135*, 1133–1143. [CrossRef]
2. Zhong, G.; Tang, Y.; Ding, X.; Chen, G.; Li, Z. Experimental investigation on wettability and capillary performance of ultrasonic modified grooved aluminum wicks. *Int. J. Heat Mass Transfer.* **2021**, *179*, 121642. [CrossRef]
3. Xie, D.; Sun, Y.; Wang, G.; Chen, S.; Ding, G. Significant factors affecting heat transfer performance of vapor chamber and strategies to promote it: A critical review. *Int. J. Heat Mass Transfer.* **2021**, *175*, 121132. [CrossRef]
4. Ji, X.; Xu, J.; Zhao, Z.; Yang, W. Pool boiling heat transfer on uniform and non-uniform porous coating surfaces. *Exp. Therm. Fluid Sci.* **2013**, *48*, 198–212. [CrossRef]
5. Scott, G.L.; Massoud, K. Pool-boiling CHF enhancement by modulated porous-layer coating: Theory and experiment. *Int. J. Heat Mass Transf.* **2001**, *44*, 4287–4311.
6. Xu, J.; Ji, X.; Zhang, W.; Liu, L. Pool boiling heat transfer of ultra-light copper foam with open cells. *Int. J. Multiph. Flow.* **2008**, *34*, 1008–1022. [CrossRef]
7. Weibel, J.A.; Garimella, S.V.; North, M.T. Characterization of evaporation and boiling from sintered powder wicks fed by capillary action. *Int. J. Heat Mass Transfer.* **2010**, *53*, 4204–4215. [CrossRef]
8. Huang, G.; Yuan, W.; Tang, Y.; Zhang, B.; Zhang, S.; Lu, L. Enhanced capillary performance in axially grooved aluminium wicks by alkaline corrosion treatment. *Exp. Therm. Fluid Sci.* **2017**, *82*, 212–221. [CrossRef]
9. Zhang, S.; Chen, G.; Jiang, X.; Li, Y.; Waqar Ali Shah, S.; Tang, Y.; Wang, Z.; Pan, C. Hierarchical gradient mesh surfaces for superior boiling heat transfer. *Appl. Therm. Eng.* **2023**, *219*, 119513. [CrossRef]
10. Ameli, M.; Agnew, B.; Leung, P.S.; Ng, B.; Sutcliffe, C.J.; Singh, J.; McGlen, R. A novel method for manufacturing sintered aluminium heat pipes (SAHP). *Appl. Therm. Eng.* **2013**, *52*, 498–504. [CrossRef]
11. Wu, Z.; Cao, Z.; Sundén, B. Saturated pool boiling heat transfer of acetone and HFE-7200 on modified surfaces by electrophoretic and electrochemical deposition. *Appl. Energy* **2019**, *249*, 286–299. [CrossRef]
12. Schaffer, G.B.; Sercombe, T.B.; Lumley, R.N. Liquid phase sintering of aluminium alloys. *Mater. Chem. Physics.* **2001**, *67*, 85–91. [CrossRef]
13. Rohsenow, V.M. *A Method of Correlating Heat Transfer Data for Surface Boiling of Liquids*; MIT Division of Industrial Cooporation: Cambridge, MA, USA, 1951; p. 31. Available online: https://dspace.mit.edu/handle/1721.1/61431 (accessed on 25 February 2023).
14. Pioro, I.L. Experimental evaluation of constants for the Rohsenow pool boiling correlation. *Int. J. Heat Mass Transfer.* **1999**, *42*, 2003–2013. [CrossRef]
15. Shibli, I.A.; Davies, D.E. Formability and electrochemical characteristics of aluminium dry powder coatings. *Mater. Sci. Technol.* **2013**, *5*, 605–608. [CrossRef]
16. Shibli, I.A.; Davies, D.E. Effect of Oxidation on Sintering Characteristics of Al Powder and Effect of Some Minor Metallic Additions. *Powder Metall.* **2013**, *30*, 97–102. [CrossRef]
17. Godinez, J.C.; Fadda, D.; Lee, J.; You, S.M. Enhancement of pool boiling heat transfer in water on aluminum surface with high temperature conductive microporous coating. *Int. J. Heat Mass Transfer.* **2019**, *132*, 772–781. [CrossRef]